



Article

# Poly Organotin Acetates against DNA with Possible Implementation on Human Breast Cancer

George K. Latsis <sup>1,\*</sup>, Christina N. Banti <sup>1,\*</sup>, Nikolaos Kourkoumelis <sup>2,\*</sup>,  
Constantina Papatriantafyllopoulou <sup>3</sup>, Nikos Panagiotou <sup>3</sup>, Anastasios Tasiopoulos <sup>3</sup>,  
Alexios Douvalis <sup>4</sup>, Angelos G. Kalampounias <sup>5</sup>, Thomas Bakas <sup>4</sup> and Sotiris K. Hadjikakou <sup>1,\*</sup>

<sup>1</sup> Section of Inorganic and Analytical Chemistry, Department of Chemistry, University of Ioannina, 45110 Ioannina, Greece; glatsis@icloud.com

<sup>2</sup> Medical Physics Laboratory, Medical School, University of Ioannina, 45110 Ioannina, Greece

<sup>3</sup> Department of Chemistry, University of Cyprus, 1678 Nicosia, Cyprus; constantina.papatriantafyllopo@nuigalway.ie (C.P.); panagiotou.nikos@ucy.ac.cy (N.P.); atasio@ucy.ac.cy (A.T)

<sup>4</sup> Mössbauer Spectroscopy and Physics of Material Laboratory, Department of Physics, University of Ioannina, 45110 Ioannina, Greece; adouval@cc.uoi.gr (A.D.); tbakas@uoi.gr (T.B.)

<sup>5</sup> Physical Chemistry Laboratory, Department of Chemistry, University of Ioannina, 45110 Ioannina, Greece; akalamp@cc.uoi.gr

\* Correspondence: cbanti@cc.uoi.gr (C.N.B.); nkourkou@uoi.gr (N.K.); shadjika@uoi.gr (S.K.H.); Tel.: +30-2651-008374 (S.K.H.)

Received: 16 June 2018; Accepted: 12 July 2018; Published: 14 July 2018



**Abstract:** Two known tin-based polymers of formula  $\{[R_3Sn(CH_3COO)]_n\}$  where R = *n*-Bu– (1) and R = Ph– (2), were evaluated for their in vitro biological properties. The compounds were characterized via their physical properties and FT-IR, <sup>119</sup>Sn Mössbauer, and <sup>1</sup>H NMR spectroscopic data. The molecular structures were confirmed by single-crystal X-Ray diffraction crystallography. The geometry around the tin(IV) ion is trigonal bi-pyramidal. Variations in O–Sn–O···Sn' torsion angles lead to zig-zag and helical supramolecular assemblies for 1 and 2, respectively. The in vitro cell viability against human breast adenocarcinoma cancer cell lines: MCF-7 positive to estrogens receptors (ERs) and MDA-MB-231 negative to ERs upon their incubation with 1 and 2 was investigated. Their toxicity has been studied against normal human fetal lung fibroblast cells (MRC-5). Compounds 1 and 2 exhibit 134 and 223-fold respectively stronger antiproliferative activity against MDA-MB-231 than cisplatin. The type of the cell death caused by 1 or 2 was also determined using flow cytometry assay. The binding affinity of 1 and 2 towards the CT-DNA was suspected from the differentiation of the viscosity which occurred in the solution containing increasing amounts of 1 and 2. Changes in fluorescent emission light of Ethidium bromide (EB) in the presence of DNA confirmed the intercalation mode of interactions into DNA of both complexes 1 and 2 which have been ascertained from viscosity measurements. The corresponding apparent binding constants ( $K_{app}$ ) of 1 and 2 towards CT-DNA calculated through fluorescence spectra are  $4.9 \times 10^4$  (1) and  $7.3 \times 10^4$  (2) M<sup>-1</sup> respectively. Finally, the type of DNA binding interactions with 1 and 2 was confirmed by docking studies.

**Keywords:** biological inorganic chemistry; acetic acid; organotins; bio-polymer; anti-cancer activity; cell cycle

## 1. Introduction

Platinum-based compounds are at the focal point of research on potent anticancer drugs since the discovery of the anticancer potential of cisplatin, back during 70's [1–4]. However, platinum-based

cancer treatments are being dominated by serious side effects [5]. Moreover, cancer cells resistance against platinum based drugs is developed in a short while [6]. Nowadays, organometallic compounds, with a different pharmacological profile than that of platinum one, are developed and tested against various types of cancer cells [7].

During the last decades the anticancer activity of organotin compounds (OTCs) has been well studied [8–29]. Therefore, the investigation of new OTCs of low toxicity and improved anticancer activity are known to induce apoptosis in several cancer cell lines [17–19]. Their activity can be coupled to the lipophilicity of alkyl or aryl groups attached to the tin atoms [21]. In addition, due to their lipophilicity, OTCs are able to permeate membranes and reach the cell nucleus, where the dissociable ligands yield intermediate molecules capable of binding DNA [16,26].

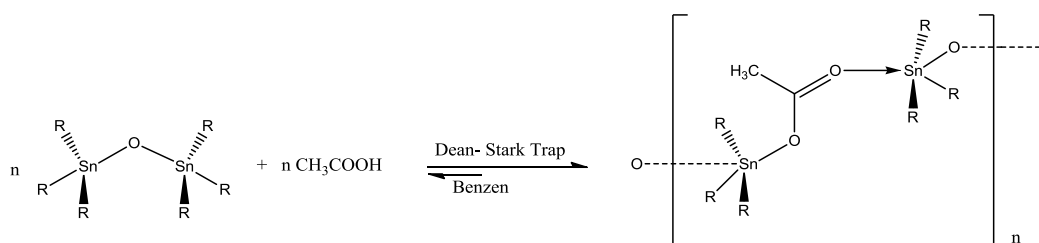
The advantages of the use of polymeric drugs as anticancer agents have been described earlier [30]. This is because: (i) the polymers overcome cellular resistance mechanisms; (ii) the polymers could be used as carriers in high-dose chemotherapy; (iii) polymers are filtered out by the kidneys more slowly than small compounds increasing the body retention time; (iv) the size and structure of the polymer provide more binding sites to cellular targets; (v) the polymers can be act as hybrid drugs incorporating multiple anticancer agents against cells through different mechanisms; and (vi) the polymers accumulate in solid tumors more than in normal tissues [30].

In the course of our studies on the design and synthesis of new metallodrugs [13–29], the known  $\{[R_3Sn(CH_3COO)]_n\}$  where R = *n*-Bu– (1) and R = Ph– (2) compounds were isolated from the reaction between acetic acid with tributyltin or triphenyltin oxides. The compounds were characterized via their physical properties and their FT-IR,  $^{119}Sn$  Mössbauer, and  $^1H$  NMR spectroscopic data, while their structures were verified by single-crystal X-Ray diffraction crystallography. The enhancement on the biological activity against tumor cells of the polymeric 1 and 2 is studied in relation to their polymeric intermolecular architecture (helical and zig-zag). The presence of acetic acid is also, expected to adjust the lipophilicity of the metallodrugs. The in vitro cell viability against MCF-7 (estrogen receptor (ER) positive) and MDA-MB-231 (estrogen receptor (ER) negative) was evaluated. Their genotoxicity has been studied against normal human fetal lung fibroblast cells (MRC-5). The type of the cell death caused by 1 and 2 was studied by flow cytometry assay. Finally, conclusions on Structure Activity Relationship are derived, in the light of the results obtained for OCT's from our group up to now.

## 2. Results and Discussion

### 2.1. General Aspects

Complexes 1 and 2 were synthesized as pale white powders by refluxing a benzene solution of tri-aryl-tin oxide and acetic acid (glacial) in a 1:1 molar ratio (Scheme 1), using a Dean–Stark water trap.



**Scheme 1.** Preparation route of 1 and 2.

The formulae of 1 and 2 were first deduced by melting point and spectroscopic data. Crystals of the complexes 1 and 2 are stable in air. Complexes 1 and 2 are soluble in DMSO, DMF, toluene, ethanol, acetone, and diethyl-ether.

## 2.2. Solid State

### 2.2.1. Vibrational Spectroscopy

The  $\nu_{\text{as}}(\text{COO}^-)$  vibrations are observed at 1584 (**1**) and 1574 (**2**)  $\text{cm}^{-1}$  respectively, while the bands at 1418 (**1**) and 1416 (**2**)  $\text{cm}^{-1}$  are assigned to  $\nu_{\text{s}}(\text{COO}^-)$  (Figure S1). The  $\Delta\nu$  [ $\nu_{\text{as}}(\text{COO}^-) - \nu_{\text{s}}(\text{COO}^-)$ ] value is 166 (**1**) and 158 (**2**)  $\text{cm}^{-1}$ , respectively. Monodentate coordination of the carboxylic group results in significantly higher difference values  $\Delta\nu$  than those observed for the ionic compounds of the ligand [20], while when the ligand chelates, the  $\Delta\nu$  is considerably smaller than that observed for its ionic compounds. For asymmetric bidentate coordination, the values are in the range of monodentate one [20]. When the  $-\text{COO}-$  group bridges metal ions, the  $\Delta\nu$  values are higher than that of the chelating mode and nearly the same as that observed for ionic compounds [20]. In the case of sodium acetate, the  $\Delta\nu$  [ $\nu_{\text{as}}(\text{COO}^-) - \nu_{\text{s}}(\text{COO}^-)$ ] value is 170  $\text{cm}^{-1}$  [31]. Since the  $\Delta\nu$  values in **1** and **2** (166 (**1**) and 158 (**2**)  $\text{cm}^{-1}$ ) is in the range of the corresponding one of sodium acetate (170  $\text{cm}^{-1}$ ) the bridging coordination mode is concluded for the carboxylic group in **1** and **2** (Figure S1). Bands at 493 (**1**) and 457 (**2**)  $\text{cm}^{-1}$  in the spectra of **1** and **2** are assigned to the  $\nu(\text{Sn}-\text{O})$  bond vibrations [20], while the corresponding bands at 672, 614 (**1**) and 730, 698 (**2**)  $\text{cm}^{-1}$  are assigned to the antisymmetric and symmetric vibrations of  $\text{Sn}-\text{C}$  bonds [29].

### 2.2.2. $^{119}\text{Sn}$ Mössbauer Spectroscopy

$^{119}\text{Sn}$  Mössbauer spectra at 80 K are shown in Figure 1.

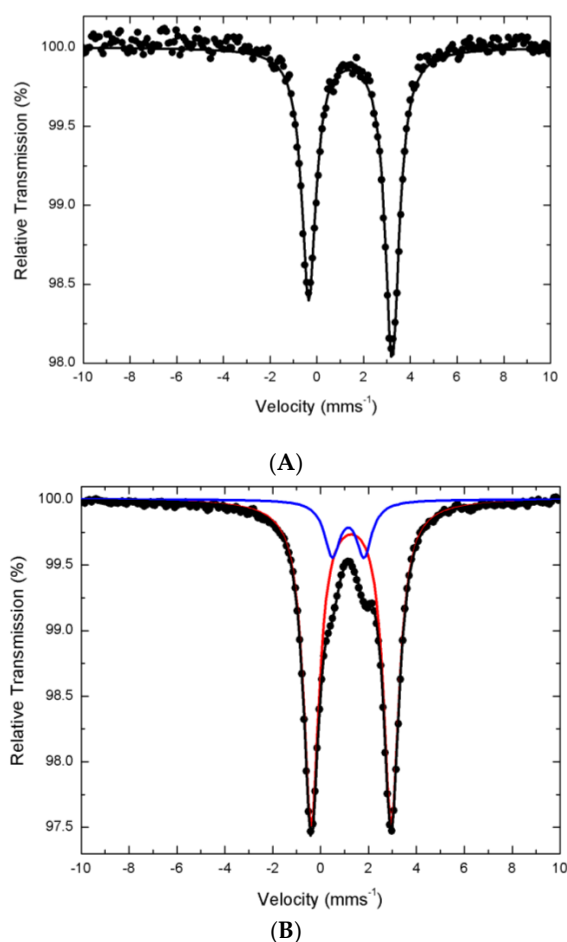


Figure 1.  $^{119}\text{Sn}$  Mössbauer spectra of **1** (A) and **2** (B) at 80 K.

The spectrum of **1** consists of one asymmetric Lorentzian doublet. The absorption line intensity asymmetry could be attributed to the recoilless fraction (*f*) asymmetry, which could be a consequence of vibrational-bond anisotropic involving the Sn ions [32]. Preferred orientation of the crystallites in the powdered sample cannot also be excluded in order to justify this asymmetry. The occurrence of one Lorentzian doublet, indicates either the existence of one type of Sn atom in **1** or one structural isomer [25,29]. The corresponding spectrum of **2** consists by two symmetric Lorentzian doublets. The occurrence of two symmetric Lorentzians, however, indicates two kinds of tin centers under different environment in **2** with 85–15% molar ratio [25,29]. The values of the Isomer Shifts (I.S.) of +1.44 (**1**), 1.28 (**2A**) and 1.15 (**2B**)  $\text{mm}\cdot\text{s}^{-1}$  corresponds to the (4+) oxidation state [25,29]. The quadrupole splitting parameter ( $\Delta E_q$ ) values are 3.57 (**1**), 3.35 (**2A**) and 1.33 (**2B**)  $\text{mm}\cdot\text{s}^{-1}$ . Therefore, trigonal-bipyramidal (tbp) geometry should be concluded for tin(IV) ions in **1** and **2A** as in the case of tbp  $\text{R}_3\text{Sn(IV)}$  (eg- $\text{R}_3$  = alkyl) geometry where the  $\Delta E_q$  values lie between 2.50–4.00  $\text{mm}\cdot\text{s}^{-1}$  [25,29]. On the contrary, tetrahedral (tet) geometry  $\text{R}_3\text{Sn(IV)}$  results in to  $\Delta E_q$  values of 1.30–3.00  $\text{mm}\cdot\text{s}^{-1}$  [25,29], tet conformation should be attributed to the tin(IV) atoms in **2B**.

### 2.2.3. Crystal and Molecular Structures of $[\text{Bu}_3\text{SnCH}_3\text{COO}]_n$ (**1**) and $[\text{Ph}_3\text{SnCH}_3\text{COO}]_n$ (**2**)

Crystals suitable for X-ray analysis were obtained by slow evaporation of diethyl-ether solutions of **1** and **2**. Their formula was confirmed here by single crystal X-ray diffraction analysis at ambient conditions. The structure of **1** is identical to that already reported by M. Adeel Saeed et. al. [33]. Thus **1** crystallizes in  $\text{P}2_1/\text{c}$  space group,  $a = 10.1845(3)$ ,  $b = 20.2542(7)$ ,  $c = 16.2466(6)$  Å,  $\beta = 94.739(3)^\circ$ ,  $V = 3339.87$  Å<sup>3</sup>; while the reported one crystallizes in  $\text{P}2_1/\text{c}$  space group,  $a = 10.386(4)$ ,  $b = 20.924(3)$ ,  $c = 16.584(6)$  Å,  $\beta = 92.87(2)^\circ$ ,  $V = 3599(2)$  Å<sup>3</sup> [33]. Although, **2** crystallizes in  $\text{Pn}$  space group with  $a = 16.7427(6)$ ,  $b = 10.0426(2)$ ,  $c = 25.5119(8)$  Å,  $\alpha = 89.999(2)$ ,  $\beta = 100.936(3)$ ,  $\gamma = 89.998(2)^\circ$ ,  $V = 4211.68$  Å<sup>3</sup>, the already reported crystallizes in  $\text{P}2_1/\text{c}$ , space group,  $a = 8.969(4)$ ,  $b = 10.146(5)$ ,  $c = 19.540(7)$  Å,  $\beta = 93.70(4)^\circ$ ,  $V = 1774.5$  Å<sup>3</sup> [34] suggesting a polymorphism between **2** and the published one. However, the extended disorder on the density observed in **2** prevent its accurate refinement allowing only qualitative conclusions to be drawn. Although the obtained X-ray data do not allow discussion about bond lengths and angles, they are of sufficient quality to determine the connectivity and the packing of **2**. The molecular diagrams of **1** and **2** are shown in Figure 2.

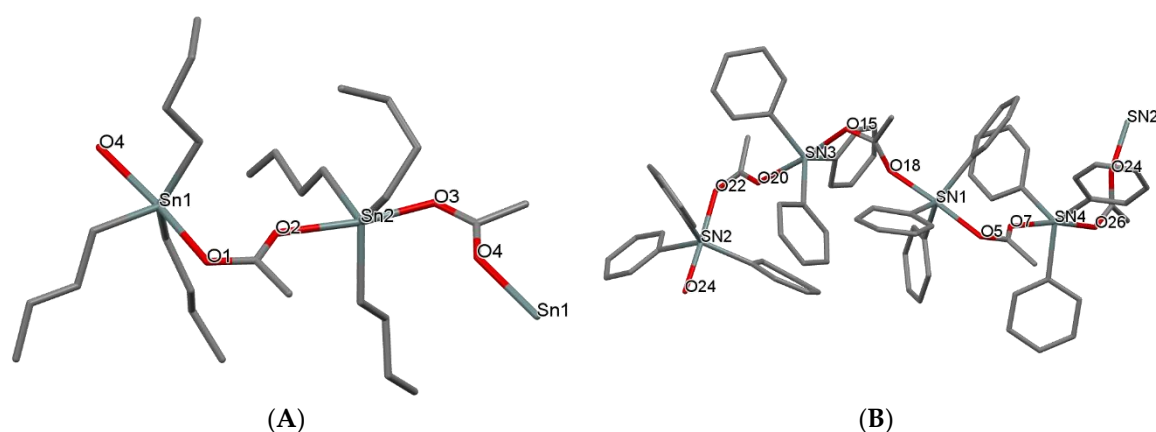
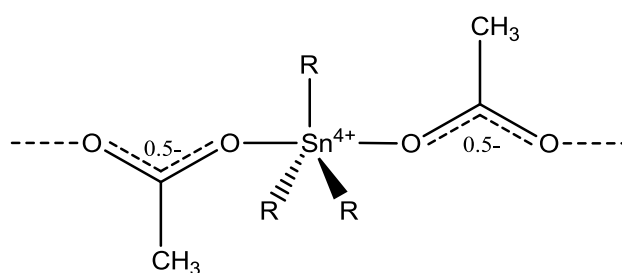


Figure 2. Molecular diagrams of **1** (A) and **2** (B).

Three C atoms from the alkyl groups and two O atoms from two de-protonated  $\text{CH}_3\text{COOH}$  molecules form the trigonal bipyramidal arrangement around the Sn ions in **1**. The average C–O bond lengths found in **1** and **2** ( $1.260 \pm 0.020$  Å), indicates a bond order of 1.5 e. This delocalization of the electron density in the  $-\text{COO}^-$  group suggests a charge distribution shown in Scheme 2.



Scheme 2. Charge distribution.

### 2.3. Solution Studies

#### <sup>1</sup>H-NMR Spectroscopy

The <sup>1</sup>H-NMR spectrum of free acetic acid in DMSO-*d*<sub>6</sub> is dominated by a single resonance signal at 1.91 (s, H) ppm for the methyl protons, which is shifted upon its coordination to the tin(IV) ion at 1.776 (s, H) ppm in **1** and at 1.758 (s, H) ppm in **2** (Figure S2). In the case of **1** four additional signals are observed at 1.52 ppm (t, H<sup>a</sup>(-<sup>a</sup>CH<sub>2</sub>-Sn)), 1.27 ppm (m, H<sup>b</sup>(-<sup>b</sup>CH<sub>2</sub>-CH<sub>2</sub>-Sn)), at 1.00 ppm (m, H<sup>c</sup>(-<sup>c</sup>CH<sub>2</sub>-CH<sub>2</sub>-CH<sub>2</sub>-Sn)), and 0.84 ppm (t, H<sup>d</sup>(<sup>d</sup>CH<sub>3</sub>-CH<sub>2</sub>-CH<sub>2</sub>-CH<sub>2</sub>-Sn)) of the butyl substituent bind on tin(IV) ions (Figure S2). These four signals (1.52–0.84 ppm) have been replaced by the signals at 7.79–7.45 ppm in the spectrum of **2** (Figure S2), which were attributed into the aromatic protons of phenyl substituent of organotin moieties. Since the cells were incubated for 48 h the stability of **1** and **2** is checked for this period with <sup>1</sup>H-NMR spectroscopy. No changes were observed between the initial spectra of freshly prepared solutions and the corresponding spectra when measured after 48 h confirming the retention of the structures in solution (Figure S2).

### 2.4. Biological Tests

#### 2.4.1. Anti-Proliferative Activity

Organotin compounds **1** and **2** were tested for their *in vitro* cytotoxic activity against human breast adenocarcinoma cell lines, MCF-7 and MDA-MB-231, by the mean of sulforhodamine B (SRB) assay [16,17]. The cells were incubated for 48 h with **1** and **2**. Since ERs are expressed in 65% of human breast cancer, (a hormone dependent malignancy) the MCF-7 and MDA-MB-231 cells were used in order to ascertain the influence of the ER's in the mechanism of action of **1** and **2** [16,17]. MCF-7 cells serve as a valuable model system to elucidate pathways of hormone response and resistance. Especially, the MCF-7 cells were used for studying estrogen response both *in vitro* and *in vivo* [35]. MDA-MB-231 human breast cancer cells, on the other hand, are used as a model of ER-negative breast cancers [36].

The IC<sub>50</sub> values of **1** and **2** against MCF-7 cells lie in the range of nM and they are 0.25 ± 0.02 and 0.21 ± 0.01 μM respectively, while their corresponding IC<sub>50</sub> values against MDA-MB-231 cells are 0.20 ± 0.01 and 0.12 ± 0.01 μM. The activity of **1** follows reverse order to the corresponding one of **2** against these cell lines suggesting no interference of the estrogen receptors to their mechanism. By taking into account the IC<sub>50</sub> value of cisplatin against MCF-7 and MDA-MB-231 cells (5.5 ± 0.4 and 26.7 ± 1.1 μM respectively), both **1** and **2** exhibit extremely cytotoxic activity against these cell lines. These values indicate 22 and 26-fold higher activity of **1** and **2** against MCF-7 cells than cisplatin and 134 and 223-fold against MDA-MB-231 cells. Despite their strong activity against tumor cells, **1** and **2** also exhibit high toxic activity against MRC-5 cells with IC<sub>50</sub> values of 0.22 ± 0.01 (**1**) and 0.11 ± 0.01 (**2**) μM, respectively. The IC<sub>50</sub> values against MCF-7, MDA-MB-231, and MRC-5 cells of organotin compounds studied from our group, are summarized in Table 1. The following conclusions are made: (i) tri-organotin derivatives are more active than the corresponding di-organotin ones; (ii) organotin derivatives of carboxylic acids are generally more active than those of other types of

ligands; (iii) organotin compounds are also highly toxic, even more toxic than cisplatin; (iv) however the selectivity index, which is defined as the IC<sub>50</sub> value against MRC-5 towards the corresponding value against MCF-7, and is an indicator of the therapeutic potency of a compound (the higher the value is, the better potency), shows that **1** and **2** are more potent therapeutics (TPI values of 0.88 (**1**) and 0.52 (**2**)) than cisplatin (TPI = 0.20). (v) The tri-*n*-butyl tin compound of thiobarbituric acid (*n*-Bu)<sub>3</sub>Sn(*o*-HTBA)(H<sub>2</sub>O) exhibits the higher TPI value of 1.6 (Table 1).

**Table 1.** Bioactivity data recorded for **1** and **2** in comparison with those of other reported organotin compounds.

Compound	IC <sub>50</sub> (μM)				Ref.
	MCF-7	MDA-MB-231	MRC-5	TPI *	
<b>1</b>	0.25 ± 0.02	0.20 ± 0.01	0.22 ± 0.01	0.88	[present]
<b>2</b>	0.21 ± 0.01	0.12 ± 0.01	0.11 ± 0.01	0.52	[present]
{[Ph <sub>3</sub> Sn] <sub>2</sub> (mna)-[(CH <sub>3</sub> ) <sub>2</sub> CO]}	0.030		>0.200		[18]
[Me <sub>2</sub> Sn(Sal) <sub>2</sub> ]	0.142 ± 0.043		0.0975 ± 0.00015	0.69	[19]
[( <i>n</i> -Bu) <sub>2</sub> Sn(Sal) <sub>2</sub> ]	0.108 ± 0.0026		0.1041 ± 0.0002	0.96	[19]
[( <i>n</i> -Bu) <sub>3</sub> Sn(Sal)]	0.724 ± 0.0054		0.0981 ± 0.0001	0.14	[19]
[Ph <sub>3</sub> Sn(Sal)]	0.121 ± 0.0037		0.0945 ± 0.0002	0.78	[19]
[( <i>n</i> -Bu) <sub>3</sub> Sn(pHbza)]	0.325 ± 0.0023		0.0784 ± 0.0002	0.24	[19]
{[Ph <sub>3</sub> Sn( <i>o</i> -HTBA)] <sub>n</sub> }	0.103	0.203	0.130	1.26	[17]
( <i>n</i> -Bu) <sub>3</sub> Sn( <i>o</i> -HTBA)(H <sub>2</sub> O)	0.068	0.106	0.108	1.59	[17]
[( <i>tert</i> -Bu) <sub>2</sub> (HO-Ph)] <sub>2</sub> SnCl <sub>2</sub>	3.12 ± 0.38				[14]
[( <i>tert</i> -Bu) <sub>2</sub> (HO-Ph)] <sub>2</sub> Sn(PMT) <sub>2</sub>	7.86 ± 0.87				[14]
[( <i>tert</i> -Bu) <sub>2</sub> (HO-Ph)] <sub>2</sub> Sn(MPMT) <sub>2</sub>	0.58 ± 0.1				[14]
{[( <i>tert</i> -Bu) <sub>2</sub> (HO-Ph)] <sub>2</sub> SnCl(PYT)}	>30				[14]
[( <i>tert</i> -Bu) <sub>2</sub> (HO-Ph)] <sub>2</sub> SnCl(MBZT)	>30				[14]
Ph <sub>3</sub> SnCl	0.130	0.166	0.141	1.08	[16]
[Ph <sub>3</sub> SnOH] <sub>n</sub>	0.070	0.165	0.090	1.29	[16]
[(Ph <sub>2</sub> Sn) <sub>4</sub> Cl <sub>2</sub> O <sub>2</sub> (OH) <sub>2</sub> ]	>10	>10	>10		[16]
Me <sub>2</sub> Sn(( <i>tert</i> -Bu) <sub>2</sub> (HO-Ph-S)) <sub>2</sub>	19.20 ± 1.70		19.50 ± 1.40	1.02	[15]
Et <sub>2</sub> Sn((( <i>tert</i> -Bu) <sub>2</sub> (HO-Ph-S)) <sub>2</sub> ) <sub>2</sub>	6.20 ± 0.80		7.30 ± 0.60	1.18	[15]
( <i>n</i> -Bu) <sub>2</sub> Sn-((( <i>tert</i> -Bu) <sub>2</sub> (HO-Ph-S)) <sub>2</sub> ) <sub>2</sub>	0.40 ± 0.06		0.61 ± 0.07	1.53	[15]
Ph <sub>2</sub> Sn((( <i>tert</i> -Bu) <sub>2</sub> (HO-Ph-S)) <sub>2</sub> ) <sub>2</sub>	6.20 ± 0.80		12.40 ± 1.40	2.00	[15]
[( <i>tert</i> -Bu) <sub>2</sub> (HO-Ph)] <sub>2</sub> Sn((( <i>tert</i> -Bu) <sub>2</sub> (HO-Ph-S)) <sub>2</sub> ) <sub>2</sub>	>30	>30	>30		[15]
Me <sub>3</sub> Sn((( <i>tert</i> -Bu) <sub>2</sub> (HO-Ph-S)) <sub>2</sub> ) <sub>2</sub>	4.90 ± 0.50		3.36 ± 0.13	0.69	[15]
Ph <sub>3</sub> Sn((( <i>tert</i> -Bu) <sub>2</sub> (HO-Ph-S)) <sub>2</sub> ) <sub>2</sub>	0.25 ± 0.03		0.22 ± 0.01	0.88	[15]
Cisplatin	5.5 ± 0.4	26.7 ± 1.1	1.1 ± 0.2	0.20	[37]

\* TPI = IC<sub>50</sub>(MRC-5)/IC<sub>50</sub>(MCF-7), mna = 2-mercapto-nicotinic acid, salH = salicylic acid, pHbzaH = *p*-Hydroxyl-benzoic acid, H<sub>2</sub>TBA = 2-thiobarbituric acid, PMTH = 2-mercapto-pyrimidine, MPMTH = 2-mercapto-4-methyl-pyrimidine, PYTH = 2-mercapto-pyridine, MBZTH = 2-mercapto-benzothiazole.

#### 2.4.2. Evaluation of Genotoxicity by Micronucleus Assay In Vitro

Micronucleus assay is a reliable and an accessible technique to evaluate the appearance of genetic damage on a cell. The detection of micronucleus (MN) indicates mutagenic, genotoxic, or teratogenic effects [37]. In the presence of exogenous genotoxic factors, the MN is formed due to the metaphase–anaphase transition of the mitotic cycle. The possible induction of micronucleus frequencies was evaluated when MRC-5 cells were treated by **1** and **2** at the concentrations of their IC<sub>50</sub> values. The micronucleus frequency in the MRC-5 cell culture without treatment is 0.91 ± 0.02%, while it is 1.0 ± 0.1% upon treatment with DMSO. However, the micronucleus frequencies are slightly increased when the cells are incubated with **1** and **2** to 2.10 ± 0.04% (**1**) and 2.19 ± 0.03% (**2**) (Figure S3). The compounds **1** and **2** show a slightly increase in micronucleus frequency in contrast to the control or to cisplatin (1.6%) at its IC<sub>50</sub> value of 26 μM [37]. Cisplatin is used as a reference control. Doxorubicin has also been used as reference control from other groups. MRC-5 cells show slight increasing MN's when they are treated with **1** and **2** than the case of cisplatin indicating higher genotoxicity indeed. However, the treatment of MRC-5 cells with 0.18 μM or 0.014 μM of doxorubicin increases the percent of micronucleus at (94.7 ± 20.0)% and (17.00 ± 1.73)%, respectively, in contrast to the control ones (15.0 ± 2.64)% [38]. Thus, despite its higher genotoxicity of **1** and **2** towards MRC-5 cells than cisplatin both exhibit significant lower MN percentage than doxorubicin a medication against tumors in humans in used. It is therefore considered that **1** and **2** are nongenotoxic substances.

### 2.4.3. Cell Cycle Studies

Internucleosomal DNA fragmentation has been described as one of the main characteristics of the apoptotic process and can be identified by a sub-G<sub>1</sub> peak on DNA frequency histograms [37]. Therefore, the apoptotic type of the cell deaths caused by the regulation of cell cycle progression because of **1** and **2** can be evaluated by flow cytometric analysis since these cells give a sub-G<sub>1</sub> peak [37]. The percentage of cells in the phases of the cell cycle was analyzed after 48 h exposure of MCF-7 cells with **1** and **2** at their IC<sub>50</sub> values.

The effect on the cell cycle which is illustrated in Figure 3, as the number of cells towards DNA content in sub-G<sub>1</sub>, G<sub>0</sub>/G<sub>1</sub>, S, and G<sub>2</sub>/M phases is caused by **1** and **2**. The untreated cells are spread in 6.1% sub-G<sub>1</sub> phase, 46.5% in G<sub>0</sub>/G<sub>1</sub>, 18.3% in S, and 28.9% in G<sub>2</sub>/M phases. After incubation of MCF-7 cells with **1** and **2**, a significant increase in the number of apoptotic cells in sub-G<sub>1</sub> phase (14.4% (**1**), 24.1% (**2**), respectively) was observed towards the control group (6.1%). In the case of **1**, the cells in G<sub>0</sub>/G<sub>1</sub> phase are reduced to 37.9%, on the contrary, with 46.5% for the untreated cells while in the case of **2**, the corresponding value decrease to 35.8%. However, the percentage of MCF-7 cells in S phase, was increased to 25.1% (**1**), 22.9% (**2**). Finally, the percentage of MCF-7 cells in G<sub>2</sub>/M phase was reduced to 22.1% (**1**) and 17.1% (**2**), respectively. In the DMSO-treated cells, the distribution in phases sub-G<sub>1</sub> (6.5%), G<sub>0</sub>/G<sub>1</sub> (42.7%), S (20.6%), and G<sub>2</sub>/M (29.5%) were similar to the corresponding ones of control cells'. All the data obtained in cell cycle studies of **1** and **2** are summarized in Table 2.

**Table 2.** Cell cycle studies data of **1** and **2**.

Description	Phases of cell cycle			
	Sub-G1	G <sub>0</sub> /G <sub>1</sub>	S	G <sub>2</sub> /M
Untreated cells	6.1%	46.5%	18.3%	28.9%
Treated cells with DMSO	6.5	42.7	20.6	29.5
<b>1</b>	14.4	37.9%	25.1	22.1
<b>2</b>	24.1	35.8%	22.9	17.1

In conclusion, **1** and **2** stimulate S-phase cell cycle arrest, thus suppressing cell proliferation by inhibiting DNA synthesis, in accordance to other anticancer agents (resveratrol, mitomycin C, and hydroxyurea) [37]. Likewise, cisplatin causes cell cycle arrest at S and G<sub>2</sub>/M phases and the percentage of MCF-7 cells in sub-G<sub>1</sub> phase is increased, exhibiting an increasing number of apoptotic cells [37]. To summarize, metal drugs of this type induce cell cycle arrest either in G<sub>0</sub>/G<sub>1</sub> or in S phase (like cisplatin), resulting in MCF-7 cell growth inhibition. Therefore, the reduced cell growth caused by **1** and **2** is attributed to the apoptotic type of cell death, in accordance to the way of action of cisplatin [37].

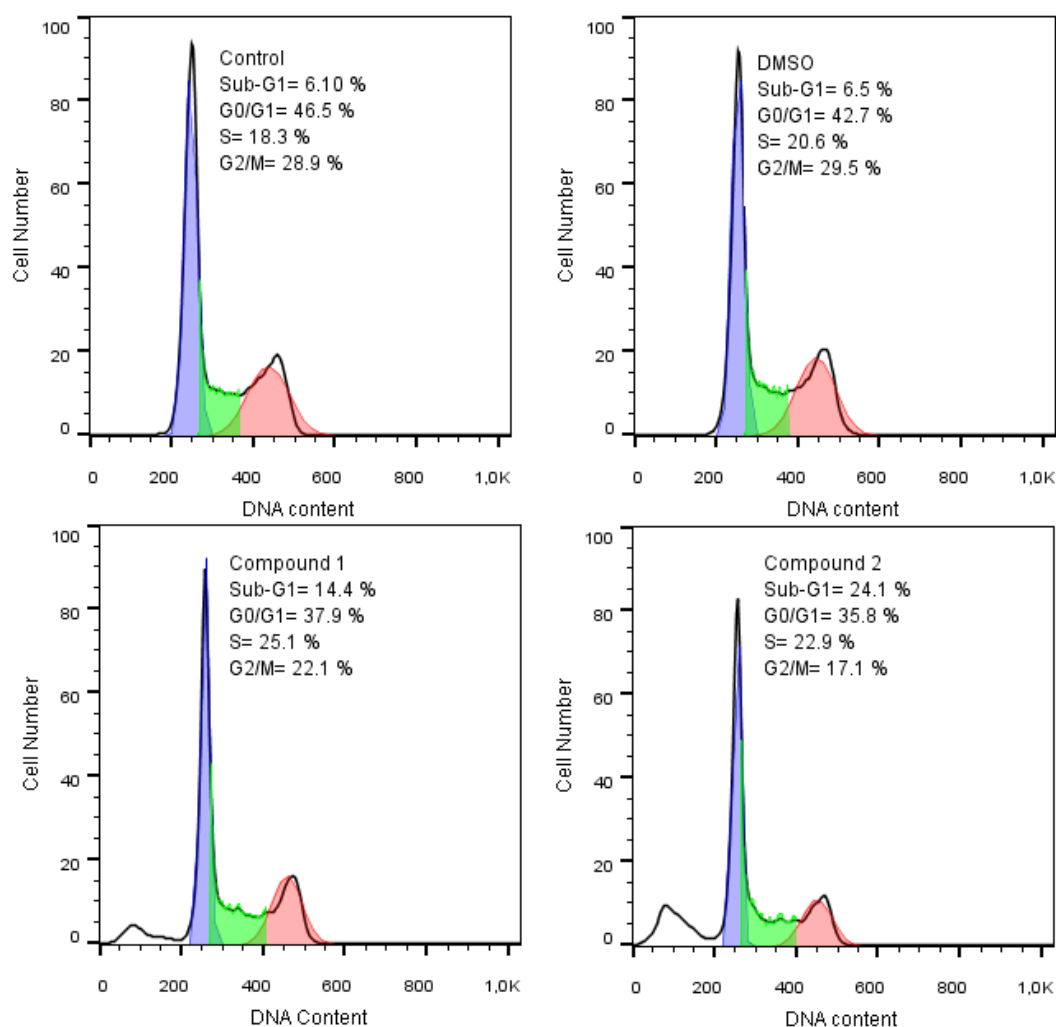


**Figure 3.** Number of MCF-7 cells in sub-G<sub>1</sub>, G<sub>0</sub>/G<sub>1</sub>, S, and G<sub>2</sub>/M phases, upon their treatment with **1** and **2**. The meaning of color labeling is white= Sub-G<sub>1</sub>, blue= G<sub>0</sub>/G<sub>1</sub>, green= S, pink= G<sub>2</sub>/M.

#### 2.4.4. Detection of the Loss of the Mitochondrial Membrane Permeabilization (MMP Assay)

The releasing of cytochrome c in the cytosol through the loss of mitochondrial membrane permeability activates the mitochondrion cell apoptosis pathway [37]. The induction of loss in mitochondrial membrane permeability in tumor cells is one of the main accomplishments of targeted chemotherapy. The MMP assay is based on the cationic hydrophobic mitochondrial potential dye which accumulates in normal mitochondria. When cells are treated with a metallo-agent, the mitochondrial membrane permeability collapses, and the fluorescence emission of the dye decreases simultaneously.

The MCF-7 cells were treated with **1** and **2** at their IC<sub>50</sub> values, for 48 h, and the fluorescence of the MMP assay dye decreased by 6.71% (**1**) and 6.52% (**2**), respectively. When the MCF-7 cells are treated with cisplatin at its IC<sub>50</sub> values (5.5 μM) the fluorescence of the MMP assay dye decreased by 54.9% [37]. Therefore, the MMP assay should not support mitochondrial membrane permeability loss. Thus, **1** and **2** cause cell death by a different mechanism. Since apoptosis has been observed from cell cycle studies, it should be activated by a different mechanism than mitochondrion pathways.

#### 2.4.5. DNA Binding Studies

DNA is the main target of the successful chemotherapeutics, the interaction of **1** and **2** towards CT-DNA was investigated by viscosity measurements and fluorescence spectroscopic studies.

(a) Viscosity measurements: DNA length changes upon its incubation with anticancer agents affect strongly affecting the viscosity of its solution. Thus (i) if the agent intercalates in the DNA strands, this results in its lengthening and a viscosity increase; (ii) if the agent interacts electrostatically with the DNA, no effect on DNA length is caused and therefore no significant change in viscosity is observed; (iii) however, in case the DNA strands are cleaved by an agent, the length of the DNA decreases, and also, the viscosity decreases significantly (iv) bending of the DNA helix caused by the agent reduces the viscosity. Therefore, viscosity exhibits high sensitivity to changes in the DNA and it is used for the study of the binding modes of an agent towards DNA [39]. The solution of CT-DNA (10 mM) is incubated with increasing amounts of **1** and **2** so that the [compound]/[DNA] molar ratio reaches  $r = 0.27$ . The relative viscosity of the solution which contains the agent/DNA/buffer, towards the corresponding one which contains DNA/buffer, increased for both compounds (Figure 4), suggesting an intercalation mode of interaction between **1** and **2** and CT-DNA.

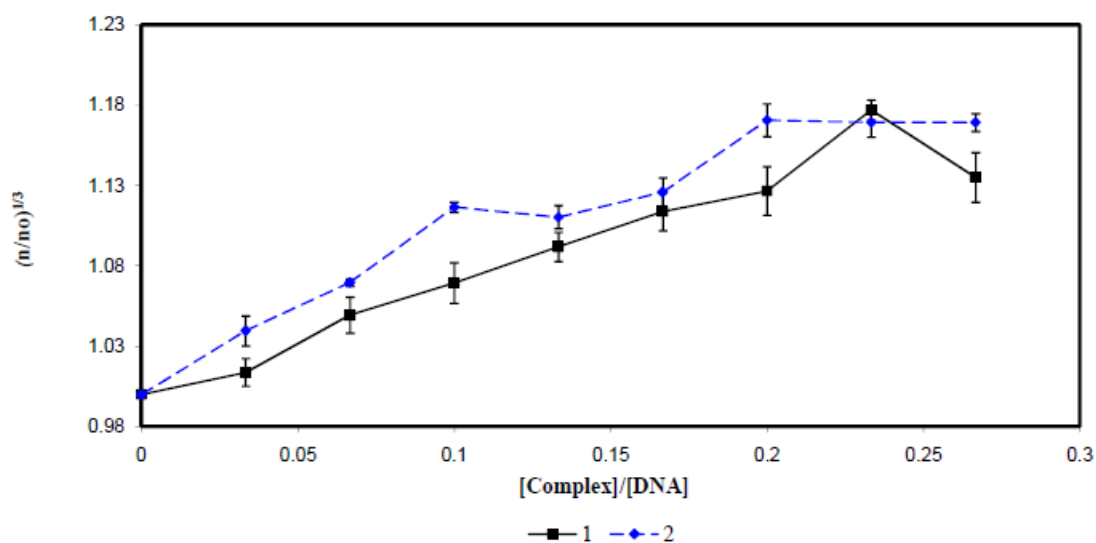


**Figure 4.** Effect of increasing concentrations of **1** and **2** on the relative viscosity of CT-DNA at 25 °C. ([DNA] = 10 mM,  $r = [\text{compound}]/[\text{DNA}]$ ,  $n$  is the viscosity of DNA in the presence of **1** or **2** and  $n_0$  is the viscosity of DNA alone).

(b) Fluorescence Spectroscopic Studies: In order to verify the intercalation mode of **1** and **2** towards CT-DNA, fluorescence spectroscopic studies were carried out. In the fluorescence spectroscopic studies the dye ethidium bromide (EB) is used. In the presence of DNA, EB emits, due to its strong intercalation between the adjacent DNA base pairs [37]. The displacement of EB during titration with the agent suggests an intercalative binding mode. The emission data of the solutions of EB with CT-DNA at 610 nm, with increasing concentrations of **1** and **2** (0–250 µM) upon their excitation at 532 nm, were recorded (Figure 5). The decreasing percent in fluorescence upon increasing of concentration of **1** and **2** at 610 nm was 31.5% (**1**) and 30.1% (**2**), respectively, confirming that both compounds can interact with DNA by the intercalation mode. The corresponding apparent binding constants ( $K_{app}$ ) of **1** and **2** towards CT-DNA calculated through fluorescence spectra are  $(4.9 \pm 0.5) \times 10^4$  (**1**) and  $(7.3 \pm 1.3) \times 10^4$  (**2**)  $M^{-1}$ , respectively, indicating stronger binding affinity of the triphenyltin than the tri-*n*-butyltin acetates.

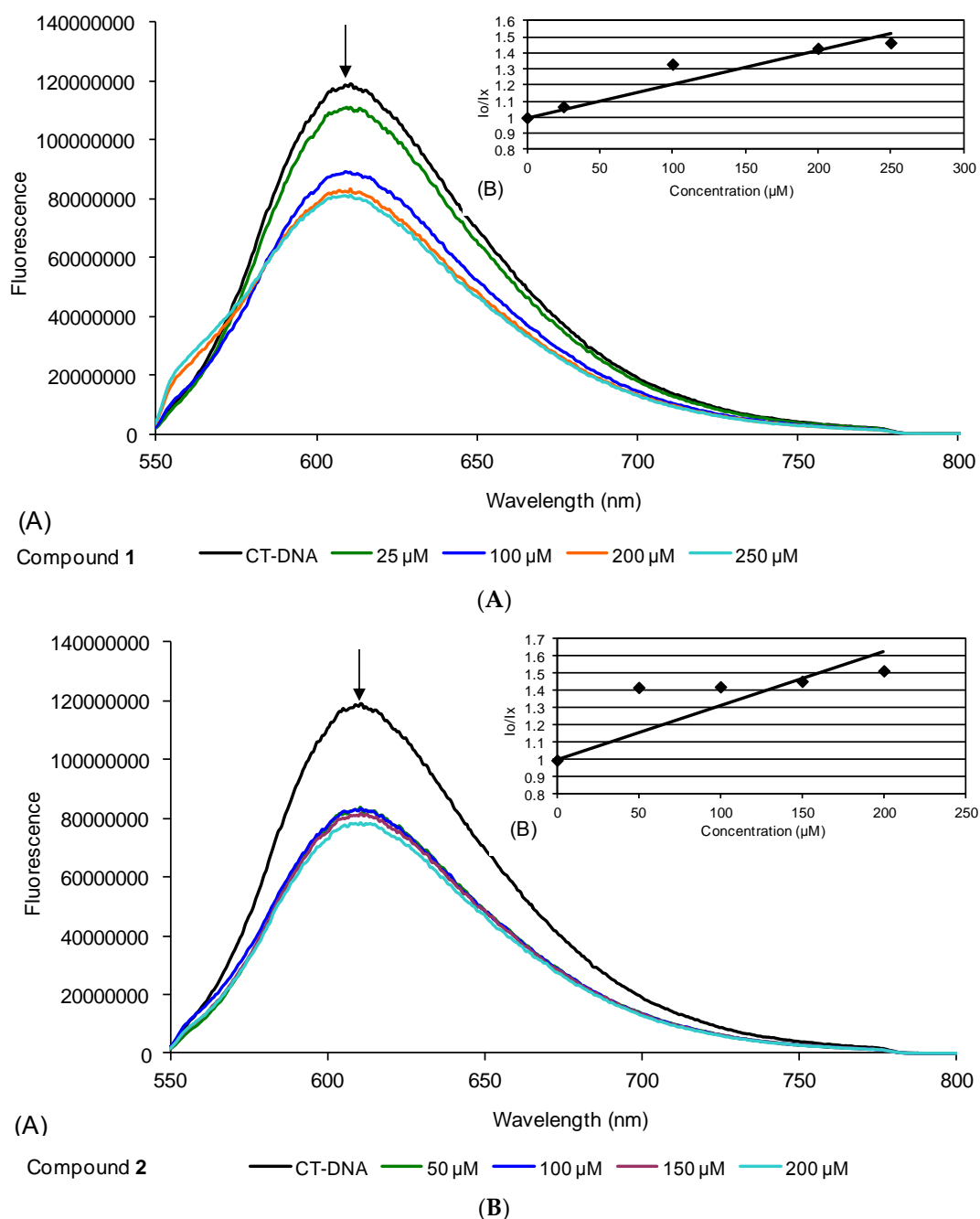


**Figure 5.** Emission spectrum of EB bound to DNA (peak around 610 nm) decreases in order of the concentration of the complex (**1 (A)** and **2 (B)**). The arrows show the intensity changing upon increasing complex concentration. Inset shows the plots of emission intensity  $I_0/I_x$  vs. [complex].

(c) Computational studies—molecular docking: In order to verify the type of interaction between DNA with **1** or **2** molecular docking calculations were performed. Small aromatic molecules can typically bind to DNA by intercalation. Generally, either a planar molecule or a fragment is inserted between two adjacent DNA base pairs to form a hydrophobic pocket in the DNA structure. This non-covalent interaction is usually stabilized by  $\pi$ -interactions; at the same time, additional interactions with the grooves are possible. Statistically, the CG intercalation site is preferable for intercalation [40]. Upon ligand binding, the DNA structure is slightly elongated and accommodates a small gap between two consecutive base pairs for the intercalators. Consequently, the latter can act as potent antitumor

drugs and mutagens, inhibiting DNA replication and transcription. Targeting DNA sequences is a challenging task for docking software, especially when intercalation sites are unavailable, because gap openings cannot be simulated with rigid receptors. Moreover, it has been shown that popular docking software fails to predict the intercalation into canonical B-DNA when analogous solved structures are lacking [41]. For these reasons, the DNA target chosen for our study was 1DSC (PDB: [www.rcsb.org](http://www.rcsb.org)) which is an octamer d(GAAGCTTC)<sub>2</sub> complexed with actinomycin D [42]. Actinomycin D is a potent antibiotic with high antibacterial and antitumor activity. It intercalates to DNA by localizing a phenoxazone ring at a GpC sequence while the two cyclic polypeptides of the drug bind to the DNA minor groove. 1DSC has been already used successfully for docking of metal complexes [43] and organic compounds [44] acting as DNA intercalators. The geometry of compounds **1** and **2** is trigonal bipyramidal (TBP) in the solid state. However, upon solvation in aqueous media their structure are converted to tetrahedral by cleavage of the Sn-O<sub>(acetate)</sub> dative bond. Tetrahedral metal complexes, unlike those with TBP geometry, can effectively bind to DNA by intercalation, although they normally cannot penetrate as deep as square planar complexes [45]. The optimized structures of the two organotin compounds [R<sub>3</sub>Sn(CH<sub>3</sub>COO)], (R = *n*-Bu (**1**), Ph- (**2**)) were used as ligands for DNA docking using AutodockVina. Molecular docking evaluates affinity potentials through a precalculated grid finding favorable binding positions for a flexible ligand towards a rigid macromolecular target. Complexes **1** and **2** were successfully docked into the B-DNA duplex and the lowest energy poses are depicted in Figure 6. The tri-phenyl derivative can adopt two different conformations intercalating in the GC region through either one phenyl-ring (Figure 6(2a)) or the carboxylic moiety (Figure 6(2b)) with computed binding free energies  $-5.5$  and  $-5.1$  kcal/mol, respectively. The planarity of the phenyl ring favors  $\pi$ - $\pi$  stacking interactions with the DNA base pairs, while additional hydrogen bonding interactions with the carboxylate O (G4:N2-Lig O, 2.97 Å and Lig O-C5O4, 3.1 Å) and with the pi-orbitals of the phenyl ring (G12:N2-Lig pi, 2.96 Å and G4:N2-Lig pi, 3.6 Å). On the other hand, the minimum energy conformation of the tri-*n*-butyl-derivative shows a semi-intercalation into the same GC region (Figure 6(1)) with lower binding affinity ( $-3.7$  kcal/mol). The structure is also stabilized by hydrogen bonding through the carboxylic moiety (G4:N2-Lig O, 3.13 Å). Possibly, the bulk and agile butyl groups significantly increase the steric hindrance and prevent the intercalation. These results support the experimental results showing that the phenyl derivative exhibits higher antitumor activity possibly through its intercalative mode of action (Table 1).

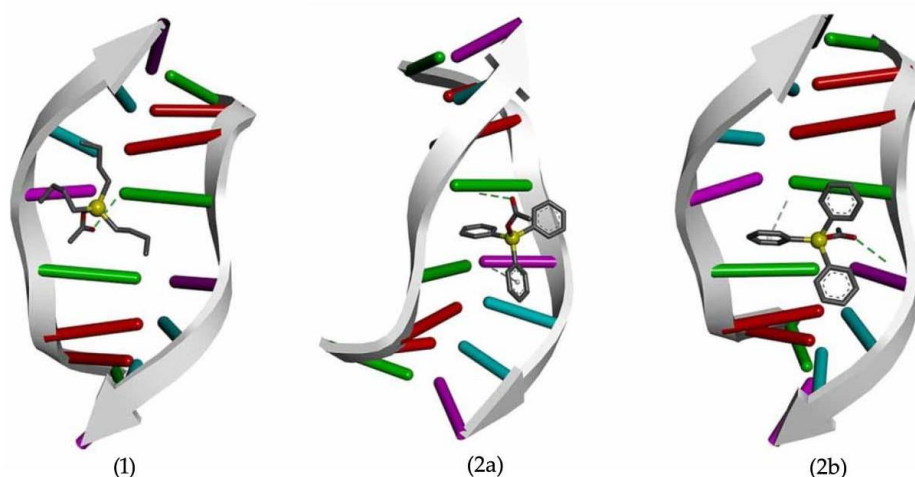


**Figure 6.** DNA docking and H-bonding interactions between B-DNA and compounds **1** and (**2a**, **2b**).

### 3. Experimental

#### 3.1. Materials and Instruments

All solvents used were of reagent grade, (Aldrich, Merck, Darmstadt, Germany) and they were used with no further purification. Infrared spectra in the region of 4000–370  $\text{cm}^{-1}$  were obtained in KBr pellets with a Jasco FT-IR-6200 spectrometer. The  $^1\text{H}$ -NMR spectra were recorded on a Bruker AC 250, 400 MHFT-NMR instrument in  $\text{DMSO-}d_6$ . Chemical shifts are given in ppm using  $^1\text{H-TMS}$  as internal reference. Elemental analysis for C, H, N, and S were carried out with a Carlo Erba EA MODEL 1108 (Waltham, MA, USA). The  $^{119}\text{Sn}$  Mössbauer spectra were collected at sample temperature of 80 K using a constant acceleration spectrometer equipped with a  $\text{Ca}^{119\text{m}}\text{SnO}_3$  source kept at room temperature. The isomer shift values of the components used to fit the spectra are given relative to  $\text{SnO}_2$  at room temperature. The  $^{119}\text{Sn}$  Mössbauer spectra were recorded with Constant acceleration WissEl-Wissenschaftliche Elektronik GmbH spectrometer (Starnberg, Germany).

#### 3.2. Synthesis and Crystallization of $\{(n\text{-Bu})_3\text{Sn}(\text{CH}_3\text{COO})\}_n$ (**1**) and $\{[\text{Ph}_3\text{Sn}(\text{CH}_3\text{COO})]_n\}$ (**2**)

Although the synthesis of these compounds is already known [33,34] we briefly described the procedure follows here. 0.5 mmol of tri-*n*-butyltin oxide ( $\text{C}_{24}\text{H}_{54}\text{OSn}_2$ , 0.298 g) for **1**, or triphenyltin(IV) hydroxide ( $\text{C}_{24}\text{H}_{16}\text{OSn}$ , 0.183 g) for **2**, were diluted with 0.5 mmol acetic acid, in 20 mL benzene in a 100-mL spherical flask. The flask was fitted with a Dean–Stark moisture trap and the reaction mixture was refluxed for 3 h. The solution was filtered and the clear filtrate was concentrated to dryness. Crystals of **1** and **2**, suitable for X-ray analysis, were formed by slow evaporation of a diethyl ether solution.

**1**: Yield: 40%; m.p: 75–76 °C; ( $\text{C}_{14}\text{H}_{30}\text{O}_2\text{Sn}$ ) $_n$  (MW = 349.04); elemental analysis: found C = 48.23, H = 6.65%; calcd: C = 48.18, H = 8.66%. MID-IR ( $\text{cm}^{-1}$ ) (KBr): 3045 w, 2330 w, 2295 s, 1959 w, 1821 w, 1659 s, 1643 w, 1573 w, 1555 s, 1428 s, 1334 vs, 1261 vs, 1077 vs, 1025 w, 997 w, 729 w, 696 w, 665 w, 609 w, 499 w, 455 w.  $^1\text{H}$  NMR (ppm) in  $\text{DMSO-}d_6$ : 1.776 (s), 1.578–1.501 (q), 1.327–1.236 (q), 1.043–1.001 (t), 0.880–0.843 (t).

**2**: Yield: 40%; m.p: 110–115 °C; ( $\text{C}_{20}\text{H}_{18}\text{O}_2\text{Sn}$ ) $_n$  (MW = 409.02); elemental analysis: found C = 58.91, H = 4.40%; calcd: C = 58.73, H = 4.43%. MID-IR ( $\text{cm}^{-1}$ ) (KBr): 2400 w, 1574 w, 1556 s, 1415 w, 1384 s, 1015 s, 867 w, 671 w, 612 s.  $^1\text{H}$  NMR (ppm) in  $\text{DMSO-}d_6$ : 7.850–7.707 (q), 7.452–7.390 (q), 1.758 (single), 1.114–1.079 (t).

#### 3.3. X-Ray Structure Determination

Single crystal X-ray diffraction data for **1** and **2** were collected on an Oxford-Diffraction Supernova diffractometer, equipped with a CCD area detector utilizing  $\text{Cu K}\alpha$  ( $\lambda = 1.5418 \text{ \AA}$ ) radiation. A suitable crystal was mounted on a Hampton cryoloop with Paratone-N oil and transferred to a goniostat where it was cooled for data collection. Empirical absorption corrections (multiscan based on symmetry-related measurements) were applied using CrysAlis RED software [46]. The structures were solved by direct methods using SIR2004 [47] and refined on  $F^2$  using full-matrix least-squares with SHELXL-2014/7 [48]. Software packages used were as follows: CrysAlis CCD for data collection [46], CrysAlis RED for cell refinement and data reduction [46], WINGX for geometric calculations [49]. The non-H atoms were treated anisotropically, whereas the aromatic H atoms were placed in calculated, ideal positions and refined as riding on their respective carbon atoms. The single crystals of compound **2** exhibited a fairly poor diffraction pattern. As a result moderate quality X-ray data were collected which did not lead to a publishable crystal structure. For this reason the X-ray data of **2** are not quoted here and have not been deposited in Cambridge Structural Database.

Supplementary data (1\_bu3sn2o\_asp\_checkcif\_new.pdf and 1\_bu3sn2o\_asp\_FINAL.cif) are available from CCDC, 12 Union Road, Cambridge CB2 1EZ, UK, (e-mail:deposit@ccdc.cam.ac.uk), on request, quoting the deposition numbers CCDC-1846946 (**1**).

**1:** (C<sub>14</sub>H<sub>30</sub>O<sub>2</sub>Sn)<sub>n</sub>: MW = 349.04, Monoclinic, space group P21/c, *a* = 10.1845(3), *b* = 20.2542(7), *c* = 16.2466(6) Å, β = 94.739(3)°, *V* = 3339.9(2) Å<sup>3</sup>, *Z* = 4, *T* = 100 K, ρ(calc) = 1.388 g·cm<sup>-3</sup>, μ = 1.522 mm<sup>-1</sup>, *F*(000) = 1440. 22782 reflections measured, 5864 unique (*R*<sub>int</sub> = 0.041), 5131 with *I* > 2σ(*I*). The final *R*<sub>1</sub> = 0.0265 (for 5131 reflections with *I* > 2σ(*I*)) and *wR*<sub>2</sub>(*F*<sup>2</sup>) = 0.0678 (all data), *S* = 1.09.

### 3.4. Biological Tests

Biological experiments were carried in dimethyl sulfoxide Dulbecco's Modified Eagle's Medium solutions (DMEM) DMSO/DMEM (0.02–0.2% *v/v*) for the complexes **1–2**. Stock solutions of the complexes **1–2**, (0.01 M) in DMSO were freshly prepared and diluted in with cell culture medium to the desired concentrations (0.05–0.4 μM). Results are expressed in terms of IC<sub>50</sub> values, which is the concentration of drug required to inhibit cell growth by 50% compared to control, after 48 h incubation of the complexes towards cell lines. Since there is no "universal" correct time point to find the IC<sub>50</sub> value of a given compound. Generally the inhibitory concentration of the 50% of the cells is determined at once at the time of the cells (of interest) doubling time, and twice the time of the doubling time. In cell culture, the vast majority of adherent cell lines display a doubling time between 18 and 24 h. In our research unit, we prefer to use 48 h since 24 h is too short to determine a reliable IC<sub>50</sub> concentration. The cell viability was determined by SRB assay as previously described [37] and it is briefly described here: Cells were plated (100 μL per well) in 96-well flat-bottom microplates at various cell inoculation densities (MCF-7, MDA-MB-231 and MRC-5: 6000, 6000 and 2000 cells/well respectively). Cells were incubated for 24 h at 37 °C and they were exposed to tested agents for 48 h afterwards, followed by the addition of an equal volume (100 μL) of complete culture medium only in the well containing the controls, or twice the final drug concentrations diluted in complete culture medium in the wells where the compounds are tested. Drug activity was measured by means of a SRB colorimetric assay giving the percent of the survival cells towards the control (untreated cells) absorbance. The culture medium was aspirated before fixation and 50 μL of 10% cold trichloroacetic acid (TCA) were gently added to the wells. Microplates were left for 30 min at 4 °C, washed five times with deionized water and left to dry at room temperature for at least 24 h. Subsequently, 70 μL of 0.4% (*w/v*) sulforhodamine B (Sigma, Darmstadt, Germany) in 1% acetic acid solution was added to each well and left at room temperature for 20 min. SRB was removed and the plates were washed five times with 1% acetic acid before air-drying. Bound SRB was solubilized with 200 μL of 10 mM un-buffered Tris-base solution. Absorbance was read in a 96-well plate reader at 540 nm.

Evaluation of genotoxicity by micronucleus assay, cell cycle studies, detection of the loss of the Mitochondrial Membrane Permeabilization (MMP assay), and fluorescence spectral studies were performed as previously reported [37]. However, they are all quoted here in brief: (a) Micronucleus: MRC-5 cells were seeded (at a density of 2 × 10<sup>4</sup> cells/well) in glass cover slips which were afterwards placed in six-well plates, with 3 mL of cell culture medium and incubate for 24 h. MRC-5 cells exposed with **1** and **2** in IC<sub>50</sub> values for a period of 48 h. After the exposure of **1** and **2**, the cover slips were washed three times with PBS and with a hypotonic solution (75 Mm KCl) for 10 min at room temperature. The hypotonized cells were fixed by at least three changes of 1/3 acetic acid/methanol. The cover slips were also washed with cold methanol containing 1% acetic acid. The cover slips were stained with acridine orange (5 μgr/mL) for 15 min at 37 °C. After, the cover slips were rinsed three times with PBS to remove any excess acridine orange stain. The number of micronucleated cells per 1000 cells was determined. (b) Cell cycle: MCF-7 cells were seeded at a density of 10<sup>5</sup> cells/well in six-well plates at 37 °C for 24 h. Cells were treated with **1** and **2** at the indicated IC<sub>50</sub> values for 48 h. The cells were then trypsinized and washed twice with phosphate-buffered saline (PBS) and separated by centrifugation. With the addition of 1 mL of cold 70% ethanol, the cells were incubated overnight at –20 °C. For analysis, the cells were centrifuged and transferred into PBS, incubated with RNase (0.2 mg/mL) and propidium iodide (0.05 mg/mL) for 40 min at 310 K and then analyzed by flow cytometry using a FACS Calibur flow cytometer (Becton Dickinson, San Jose, CA, USA). For each

sample, 10,000 events were recorded. The resulting DNA histograms were drawn and quantified using the FlowJo software (version FlowJo X 10.0.7r2, Tree Star, Ashland OR, USA). (c) Detection of the loss of the Mitochondrial Membrane Permeabilization: MCF-7 cells were treated with **1** and **2** at IC<sub>50</sub> values. After 48 h of incubation period of **1** and **2**, the cell medium was removed and added the Dye Loading Solution. The cells were incubated in 5% CO<sub>2</sub> at 37 °C for 30 min. Afterwards, 50 µL of Assay Buffer B was added of each well and are incubated for 30 min. The fluorescence intensity is measured at λ<sub>ex</sub> = 540 and λ<sub>em</sub> = 590 nm. The MMP assay kit used was purchased from sigma Aldrich “Mitochondria Membrane Potential Kit for Microplate Readers, MAK147”. (d) Fluorescent studies: The fluorescence spectroscopy method using ethidium bromide (EB) was employed to determine the relative DNA binding properties of complexes **1** and **2** into CT-DNA. The emission data at 610 nm of the spectra of EB (2.3 µM) solutions which contain CT-DNA (26 µM) in the absence or presence of various concentrations of complexes **1** and **2** (0–250 µM) were recorded upon their excitation at 532 nm (Figure 5). The apparent binding constant (K<sub>app</sub>) was calculated using the equation:

$$K_{EB}[EB] = K_{app}[\text{drug}] \quad (9)$$

where [drug] is the concentration of the complex at a 50% reduction of the fluorescence, K<sub>EB</sub> = 10<sup>7</sup> M<sup>-1</sup>, and [EB] = 2.3 µM. The concentration of the drug at a 50% reduction of the fluorescence is calculated from the diagram I<sub>0</sub>/I vs. the concentration of the complex [Q] (Figure 5), where, I<sub>0</sub> and I are the fluorescence intensities of the CT-DNA in the absence and presence of complexes **1** and **2**, respectively.

The fitting of the experimental I<sub>0</sub>/I<sub>x</sub> ratio as a function of concentration (C) was performed utilizing the linear least-squares fitting algorithm. However, the fitting procedure depends strongly on the weighting of the data points, i.e., on the knowledge of the standard deviation (SD) of every point in the experimental spectrum (<1%) since all spectra represent the average of 5000 individually recorded spectra. As a measure for the goodness of the fit, we used the R<sup>2</sup> statistics.

The slope of the I<sub>0</sub>/I<sub>x</sub> ratio as a function of C was estimated equal to a<sub>1</sub> = 2100.9 ± 204.8 and a<sub>2</sub> = 3142.4 ± 561.4 for **1** and **2** case, respectively.

The SD of the K<sub>app</sub> is calculated using the standard error propagation variance formula [50]:

$$s_f = \sqrt{\left(\frac{\partial f}{\partial x}\right)^2 (s_x)^2 + \left(\frac{\partial f}{\partial y}\right)^2 (s_y)^2 + \left(\frac{\partial f}{\partial z}\right)^2 (s_z)^2 + \dots}$$

In general, s<sub>f</sub> represents the standard deviation of the function f, s<sub>x</sub> represents the standard deviation of x, s<sub>y</sub> represents the standard deviation of y, and so forth. This formula is based on the linear characteristics of the gradient of f and therefore it is a good estimation for the standard deviation of f. Using the above methodology, the parameter K<sub>app</sub> is calculated as 48,950.97 ± 4771.84 and 73,217.92 ± 13,080.62 M<sup>-1</sup> for **1** and **2**, respectively. More details concerning the calculation of R<sup>2</sup>, the error propagation issue and other statistical parameters, see e.g., reference [50]

### 3.5. Viscosity Measurements

The kinematic viscosity of **1** and **2** was measured with the use of an Ubbelohde-type glass capillary viscosity-meter. The value of kinematic viscosity was measured as an average from triplicate measurements of viscosity with an accuracy of 2% at constant temperature. Temperature was set at 298 K by means of an ultra-thermostat.

### 3.6. Computational Studies—Molecular Docking

Molecular docking studies were carried out with AutodockVina [51] along with the graphical interface AutodockTools (ADT 1.5.6) [52] using the Lamarckian genetic algorithm (LGA). The DNA structure (PDB file 1DSC) was considered as a rigid target while no torsional restraints were applied to the complexes. Docking was performed to the optimized organotin derivatives [R<sub>3</sub>Sn(CH<sub>3</sub>COO)],

(R = *n*-Bu (1), Ph- (2)) at the B3LYP/3-21G\*/LANL2DZ(Sn) level using the Gaussian03W software package [53]. Prior to docking, water molecules and the co-crystallized ligand were removed. The search space was set as a grid box of 40 × 30 × 40 Å and spacing of 1 Å centered at the CG rich area. Default parameters were used as described in the Vina manual except from “exhaustiveness” which was set to 24.

#### 4. Conclusions

The discovery of the antitumor activity of organotin compounds goes back to the 1980s when Gielen first reports on the subject [8,9,11,12]. Later on, the antitumor properties of organotin compounds were reviewed by Saxena and Hubert [10] and Hadjiliadis et al. [13]. Continuing our studies on the antitumor activity of organotin compounds, two known compounds of formula  $\{[R_3Sn(CH_3COO)]_n\}$  where R = *n*-Bu- (1) and R = Ph (2) with trigonal bipyramidal geometry around each metal center, were used to investigate their antitumor activity against MCF-7 (positive to ERs) and MDA-MB-231 (negative to ERs). The mechanism of their action against human breast tumor cells was also investigated. Compounds 1 and 2 inhibit strongly both cell lines, while their IC<sub>50</sub> values are in nanomolar range (Table 1). The estrogen receptors play no significant role in their action. It is also concluded that (i) the tri-organotin derivatives exhibit stronger activity than the corresponding di-organotin ones (Table 1); (ii) the organotin derivatives of carboxylic acids are generally more active than those of other type of ligands (Table 1); (iii) organotin compounds are also highly toxic against normal MRC-5 cells (Table 1); (iv) the selectivity index, however, shows that 1 and 2 are more potent therapeutics (TPI values of 0.88(1) and 0.52(2)) than cisplatin (TPI = 0.20) (Table 1) and (v) among all organotins tested from our group the strongest activity against MCF-7 cells has been obtained from the triphenyltin derivative of 2-mercapto-nicotinic acid  $\{[Ph_3Sn]_2(mna) \cdot [(CH_3)_2CO]\}$  (IC<sub>50</sub> = 30 nM) and the tri-*n*-butyl tin compound of thiobarbituric acid (*n*-Bu)<sub>3</sub>Sn(o-HTBA)(H<sub>2</sub>O) (IC<sub>50</sub> = 68 nM and TPI = 1.6) (Table 1). The mitochondrial membrane permeability loss is not supported by MMP assay. Since 1 and 2 are acting through apoptosis on tumor cells (cell cycle studies) this should therefore be activated through a different pathway than that of the mitochondrion, such as the extrinsic apoptotic pathway or direct interaction with DNA. The relative viscosity measurements and fluorescence spectroscopic studies of DNA solutions suggest an intercalation mode of interaction between 1 and 2 and CT-DNA. Docking studies verify the intercalative mode, while the bulk and agile *n*-butyl groups significantly increase the steric hindrance prohibiting the intercalation, resulting in higher antitumor activity of the phenyl derivative instead of the corresponding *n*-Bu- (Table 1).

**Supplementary Materials:** Supplementary materials can be found at <http://www.mdpi.com/1422-0067/19/7/2055/s1>.

**Author Contributions:** Conceptualization, S.K.H.; Methodology, C.N.B., N.K., and S.K.H.; Validation, S.K.H., A.T., and T.B.; Investigation, G.K.L., C.N.B., N.K., C.P., N.P. A.D., and A.G.K.; Writing-Original Draft Preparation, C.N.B., N.K., and S.K.H.; Writing-Review & Editing, S.K.H.; Supervision, S.K.H.

**Funding:** This research received no external funding.

**Acknowledgments:** (i) This work was carried out in partial fulfilment of the requirements for the graduate studies of G.L. under the supervision of S.K.H. The International Graduate Program in “Biological Inorganic Chemistry”, which operates at the University of Ioannina within the collaboration of the Departments of Chemistry of the Universities of Ioannina, Athens, Thessaloniki, Patras, Crete, and the Department of Chemistry of the University of Cyprus, is acknowledged for the stimulating discussions forum. (ii) C.N.B. and S.K.H. would like to thank the Unit of Bioactivity Testing of Xenobiotics, of the University of Ioannina, for providing access to the facilities. (iii) C.N.B. and S.K.H. would like to thank the Atherothrombosis Research Centre of the University of Ioannina for providing access to the fluorescence microscope and flow cytometry. (iv) A.G.K. acknowledges the Laser Center of Ioannina University for the access to its infrastructure. S. Kaziannis (Lecturer) is also acknowledged by A.G.K. for his useful assistance during the luminescence experiments.

**Conflicts of Interest:** The authors declare no conflicts of interest.

## References

1. Rosenberg, B. Platinum coordination complexes in cancer chemotherapy. *Die Naturwissenschaften* **1973**, *60*, 399–406. [[CrossRef](#)] [[PubMed](#)]
2. Lippert, B. Impact of Cisplatin on the recent development of Pt coordination chemistry: A case study. *Coord. Chem. Rev.* **1999**, *182*, 263–295. [[CrossRef](#)]
3. Arnesano, F.; Natile, G. Mechanistic insight into the cellular uptake and processing of cisplatin 30 years after its approval by FDA. *Coord. Chem. Rev.* **2009**, *253*, 2070–2081. [[CrossRef](#)]
4. Arnesano, F.; Pannunzio, A.; Natile, G. Effect of chirality in platinum drugs. *Coord. Chem. Rev.* **2015**, *284*, 286–297. [[CrossRef](#)]
5. Astolfi, L.; Ghiselli, S.; Guaran, V.; Chicca, M.; Simoni, E.; Olivetto, E.; Lelli, G.; Martini, A. Correlation of adverse effects of cisplatin administration in patients affected by solid tumours: A retrospective evaluation. *Oncol. Rep.* **2013**, *29*, 1285–1292. [[CrossRef](#)] [[PubMed](#)]
6. Galluzzi, L.; Senovilla, L.; Vitale, I.; Michels, J.; Martins, I.; Kepp, O.; Castedo, M.; Kroemer, G. Molecular mechanisms of cisplatin resistance. *Oncogene* **2012**, *31*, 1869–1883. [[CrossRef](#)] [[PubMed](#)]
7. Huang, K.-B.; Wang, F.-Y.; Tang, X.-M.; Feng, H.-W.; Chen, Z.-F.; Liu, Y.-C.; Liu, Y.-N.; Liang, H. Organometallic Gold(III) Complexes Similar to Tetrahydroisoquinoline Induce ER-Stress-Mediated Apoptosis and Pro-Death Autophagy in A549 Cancer Cells. *J. Med. Chem.* **2018**, *61*, 3478–3490. [[CrossRef](#)] [[PubMed](#)]
8. Haiduc, I.; Silvestru, C.; Gielen, M. Organotin compounds: New organometallic derivatives exhibiting anti-tuequr activity. *Bull. Soc. Chim. Belg.* **1983**, *92*, 187–189. [[CrossRef](#)]
9. Gielen, M.; Melotte, M.; Atassi, G.; Wrllem, R. Synthesis, characterization and antitumour activity of 7,7-di-n-butyl-5,9-dioxo-6,6-dioxo-7-stanna-spiro[3,5]nonane, a di-n-butyltin(IV) analog of “paraplatin”, and of a series of di-n-butyltin(IV) derivatives of mono- and disubstituted malonic acids. *Tetrahedron* **1989**, *45*, 1219–1229. [[CrossRef](#)]
10. Saxena, A.K.; Huber, F. Organotin compounds and cancer chemotherapy. *Coord. Chem. Rev.* **1989**, *95*, 109–112. [[CrossRef](#)]
11. Gielen, M. Tin-based antitumour drugs. *Coord. Chem. Rev.* **1996**, *151*, 41–51. [[CrossRef](#)]
12. Gielen, M. Organotin compounds and their therapeutic potential: A report from the Organometallic Chemistry Department of the Free University of Brussels. *Appl. Organomet. Chem.* **2002**, *16*, 481–494. [[CrossRef](#)]
13. Hadjikakou, S.K.; Hadjiliadis, N. Antiproliferative and anti-tumor activity of organotin compounds. *Coord. Chem. Rev.* **2009**, *253*, 235–249. [[CrossRef](#)]
14. Shpakovsky, D.B.; Banti, C.N.; Beaulieu-Houle, G.; Kourkoumelis, N.; Hadjikakou, S.K.; Manoli, M.; Manos, M.J.; Tasiopoulos, A.J.; Milaeva, E.R.; Charalabopoulos, K.; et al. Synthesis, structural characterization and in vitro inhibitory studies against human breast cancer of the bis-(2,6-di-tert-butylphenol)tin(IV) dichloride and its complexes. *Dalton Trans.* **2012**, *41*, 14568–14582. [[CrossRef](#)] [[PubMed](#)]
15. Shpakovsky, D.B.; Banti, C.N.; Mukhatova, E.M.; Gracheva, Y.A.; Osipova, V.P.; Berberova, N.T.; Albov, D.V.; Antonenko, T.A.; Aslanov, L.A.; Milaeva, E.R.; et al. Synthesis, antiradical activity and in vitro cytotoxicity of novel organotin complexes based on 2,6-di-tert-butyl-4-mercaptophenol. *Dalton Trans.* **2014**, *43*, 6880–6890. [[CrossRef](#)] [[PubMed](#)]
16. Balas, V.I.; Banti, C.N.; Kourkoumelis, N.; Hadjikakou, S.K.; Geromichalos, G.D.; Sahpazidou, D.; Male, L.; Hursthouse, M.B.; Bednarz, B.; Kubicki, M.; et al. Structural and in vitro biological studies of organotin(IV) precursors; selective inhibitory activity against human breast cancer cells, positive to estrogen receptors. *Austr. J. Chem.* **2012**, *65*, 1625–1637. [[CrossRef](#)]
17. Balas, V.I.; Verginadis, I.I.; Geromichalos, G.D.; Kourkoumelis, N.; Male, L.; Hursthouse, M.B.; Repana, K.H.; Yiannaki, E.; Charalabopoulos, K.; Bakas, T.; et al. Synthesis, structural characterization and biological studies of the triphenyltin(IV) complex with 2-thiobarbituric acid. *Eur. J. Med. Chem.* **2011**, *46*, 2835–2844. [[CrossRef](#)] [[PubMed](#)]

18. Verginadis, I.I.; Karkabounas, S.; Simos, Y.; Kontargiris, E.; Hadjidakou, S.K.; Batistatou, A.; Evangelou, A.; Charalabopoulos, K. Anticancer and cytotoxic effects of a triorganotin compound with 2-mercapto-nicotinic acid in malignant cell lines and tumor bearing Wistar rats. *Eur. J. Pharm. Sci.* **2011**, *42*, 253–261. [[CrossRef](#)] [[PubMed](#)]
19. Agiorgiti, M.S.; Evangelou, A.; Vezyraki, P.; Hadjidakou, S.K.; Kalfakakou, V.; Tsanaktsidis, I.; Batistatou, A.; Zelovitis, J.; Simos, Y.V.; Ragos, V.; et al. Cytotoxic effect, antitumour activity and toxicity of organotin derivatives with ortho- or para-hydroxy-benzoic acids. *Med. Chem. Res.* **2018**, *27*, 1122–1130. [[CrossRef](#)]
20. Abdellah, M.A.; Hadjidakou, S.K.; Hadjiliadis, N.; Kubicki, M.; Bakas, T.; Kourkoumelis, N.; Simos, Y.V.; Karkabounas, S.; Barsan, M.M.; Butler, I.S. Synthesis, characterization, and biological studies of organotin(IV) derivatives with o- or p-hydroxybenzoic acids. *Bioinorg. Chem. Appl.* **2009**, *12*. [[CrossRef](#)] [[PubMed](#)]
21. Xanthopoulou, M.N.; Hadjidakou, S.K.; Hadjiliadis, N.; Milaeva, E.R.; Gracheva, J.A.; Tyurin, V.-Y.; Kourkoumelis, N.; Christoforidis, K.C.; Metsios, A.K.; Karkabounas, S.; et al. Biological studies of new organotin(IV) complexes of thioamide ligands. *Eur. J. Med. Chem.* **2008**, *43*, 327–335. [[CrossRef](#)] [[PubMed](#)]
22. Balas, V.I.; Hadjidakou, S.K.; Hadjiliadis, N.; Kourkoumelis, N.; Light, M.E.; Hursthouse, M.; Metsios, A.K.; Karkabounas, S. Crystal structure and antitumor activity of the novel zwitterionic complex of tri-*n*-butyltin(IV) with 2-thiobarbituric acid. *Bioinorg. Chem. Appl.* **2008**, 654137. [[CrossRef](#)] [[PubMed](#)]
23. Xanthopoulou, M.N.; Hadjidakou, M.N.; Hadjiliadis, N.; Kourkoumelis, N.; Milaeva, E.R.; Gracheva, J.A.; Tyurin, V.-Y.; Verginadis, I.I.; Karkabounas, S.; Baril, M.; et al. Biological studies of organotin(IV) complexes with 2-mercaptopyrimidine. *Russ. Chem. B* **2007**, *56*, 767–773. [[CrossRef](#)]
24. Xanthopoulou, M.N.; Hadjidakou, S.K.; Hadjiliadis, N.; Kubicki, M.; Karkabounas, S.; Charalabopoulos, K.; Kourkoumelis, N.; Bakas, T. Synthesis and characterization of a new chloro-di-phenyltin(IV) complex with 2-mercapto-nicotinic acid: Study of its influence upon the catalytic oxidation of linoleic acid to hydroperoxylinoleic acid by the enzyme lipoxygenase. *J. Organomet. Chem.* **2006**, *691*, 1780–1789. [[CrossRef](#)]
25. Xanthopoulou, M.N.; Hadjidakou, S.K.; Hadjiliadis, N.; Schurmann, M.; Jurkschat, K.; Michaelides, A.; Skoulika, S.; Bakas, T.; Binolis, J.; Karkabounas, S.; et al. Synthesis, structural characterization and in vitro cytotoxicity of organotin(IV) derivatives of heterocyclic thioamides, 2-mercaptobenzothiazole, 5-chloro-2-mercaptobenzothiazole, 3-methyl-2-mercaptobenzothiazole and 2-mercaptonicotinic acid. *J. Inorg. Biochem.* **2003**, *96*, 425–434. [[CrossRef](#)]
26. Banti, C.N.; Gkaniatsou, E.I.; Kourkoumelis, N.; Manos, M.J.; Tasiopoulos, A.J.; Bakas, T.; Hadjidakou, S.K. Assessment of organotin(IV) complexes against the linoleic acid, glutathione and CT-DNA. *Inorg. Chim. Acta* **2014**, *423*, 98–106. [[CrossRef](#)]
27. Xanthopoulou, M.N.; Kourkoumelis, N.; Hadjidakou, S.K.; Hadjiliadis, N.; Kubicki, M.; Karkabounas, S.; Bakas, T. Structural and biological studies of organotin(IV) derivatives with 2-mercapto-benzoic acid and -mercapto-4-methyl-pyrimidine. *Polyhedron* **2008**, *27*, 3318–3324. [[CrossRef](#)]
28. Hadjidakou, S.K.; Jurkschat, K.; Schurmann, M. Novel organotin(IV) compounds derived from bis(organostannyl)methanes: Synthesis and crystal structures of bis[diphenyl(pyridin-2-onato)stannyl]methane and bis[bromophenyl(pyrimidine-2-thionato) stannyl]methane C<sub>7</sub>H<sub>8</sub>. *J. Organomet. Chem.* **2006**, *691*, 1637–1642. [[CrossRef](#)]
29. Xanthopoulou, M.N.; Hadjidakou, S.K.; Hadjiliadis, N.; Kubicki, M.; Skoulika, S.; Bakas, T.; Baril, M.; Butler, I.S. Synthesis, structural characterization, and biological studies of six and five-coordinate organotin(IV) Complexes with the Thioamides 2-Mercaptobenzothiazole, 5-Chloro-2-mercaptobenzothiazole, and 2-Mercaptobenzoxazole. *Inorg. Chem.* **2007**, *46*, 1187–1195. [[CrossRef](#)] [[PubMed](#)]
30. Carraher, C.E., Jr.; Roner, M.R. Organotin polymers as anticancer and antiviral agents. *J. Org. Chem.* **2014**, *751*, 67–82. [[CrossRef](#)]
31. Jones, L.H.; McLaren, E. Infrared Spectra of CH<sub>3</sub>COONa and CD<sub>3</sub>COONa and Assignments of Vibrational Frequencies. *J. Chem. Phys.* **1954**, *22*, 1796–1800. [[CrossRef](#)]
32. Greenwood, N.N.; Gibb, T.C. *Mossbauer Spectroscopy*; Chapman and Hall: London, UK, 1971.
33. Saeed, M.A.; Badshah, A.; Rauf, M.K.; Craig, D.C.; Ali, S. catena-Poly[tributyltin(IV)-l-acetato]. *Acta Cryst.* **2006**, *E62*, m469–m471. [[CrossRef](#)]
34. Molloy, K.C.; Purcell, T.G.; Quill, K. Organotin biocides 1. The structure of triphenyltin acetate. *J. Organomet. Chem.* **1984**, *267*, 237–241. [[CrossRef](#)]
35. Lee, A.V.; Oesterreich, S.; Davidson, N.E. MCF-7 Cells—Changing the Course of Breast Cancer Research and Care for 45 Years. *JNCI J. Nat. Cancer Inst.* **2015**, *107*, Djv073. [[CrossRef](#)] [[PubMed](#)]

36. Rochefort, H.; Glondu, M.; Sahla, M.E.; Platet, N.; Garcia, M. How to target estrogen receptor-negative breast cancer? *Endocr. Relat. Cancer* **2003**, *10*, 261–266. [[CrossRef](#)] [[PubMed](#)]
37. Banti, C.N.; Papatriantafyllopoulou, C.; Manoli, M.; Tasiopoulos, A.J.; Hadjikakou, S.K. Nimesulide silver metallodrugs, containing the mitochondriotropic, triaryl derivatives of pnictogen; Anticancer activity against human breast cancer cells. *Inorg. Chem.* **2016**, *55*, 8681–8696. [[CrossRef](#)] [[PubMed](#)]
38. HCilião, L.; Ribeiro, D.L.; Camargo-Godoy, R.B.O.; Specian, A.F.L.; Serpeloni, J.M.; Cólus, I.M.S. Cytotoxic and genotoxic effects of high concentrations of the immunosuppressive drugs cyclosporine and tacrolimus in MRC-5 cells. *Exp. Toxicol. Pathol.* **2015**, *67*, 179–187.
39. Gao, E.; Lin, L.; Liu, L.; Zhu, M.; Wang, B.; Gao, X. Two new palladium(II) complexes: Synthesis, characterization and their interaction with HeLa cells. *Dalton Trans.* **2012**, *41*, 11187–11194. [[CrossRef](#)] [[PubMed](#)]
40. Boer, D.R.; Canals, A.; Coll, M. DNA-binding drugs caught in action: The latest 3D pictures of drug-DNA complexes. *Dalton Trans.* **2009**, 399–414. [[CrossRef](#)] [[PubMed](#)]
41. Gilad, Y.; Hanoch, S. Docking studies on DNA intercalators. *J. Chem. Inf. Model.* **2013**, *54*, 96–107. [[CrossRef](#)] [[PubMed](#)]
42. Lian, C.; Robinson, H.; Wang, A.-H. Structure of actinomycin D bound with (GAAGCTTC)<sub>2</sub> and (GATGCTTC)<sub>2</sub> and its binding to the (CAG)<sub>n</sub>:(CTG)<sub>n</sub> triplet sequence as determined by NMR analysis. *J. Am. Chem. Soc.* **1996**, *118*, 8791–8801. [[CrossRef](#)]
43. Icsel, C.; Yilmaz, V.T.; Kaya, Y.; Samli, H.; Harrison, W.T.A.; Buyukgungor, O. New palladium (II) and platinum (II) 5, 5-diethylbarbiturate complexes with 2-phenylpyridine, 2, 2'-bipyridine and 2, 2'-dipyridylamine: Synthesis, structures, DNA binding, molecular docking, cellular uptake, antioxidant activity and cytotoxicity. *Dalton Trans.* **2015**, *44*, 6880–6895. [[CrossRef](#)] [[PubMed](#)]
44. Lauria, A.; Patella, C.; Dattolo, G.; Almerico, A.M. Design and Synthesis of 4-Substituted Indolo [3, 2-e][1, 2, 3] triazolo [1, 5-a] pyrimidine Derivatives with Antitumor Activity. *J. Med. Chem.* **2008**, *51*, 2037–2046. [[CrossRef](#)] [[PubMed](#)]
45. Pages, B.J.; Ang, D.L.; Wright, E.P.; Aldrich-Wright, J.R. Metal complex interactions with DNA. *Dalton Trans.* **2015**, *44*, 3505–3526. [[CrossRef](#)] [[PubMed](#)]
46. Oxford Diffraction. *CrysAlis CCD and CrysAlis RED*; Oxford Diffraction Ltd.: Abingdon, UK, 2008.
47. Burla, M.C.; Caliendo, R.; Camalli, M.; Carrozzini, B.; Cascarano, G.L.; de Caro, L.; Giacovazzo, C.; Polidori, G.; Spagna, R. SIR2004: An improved tool for crystal structure determination and refinement. *J. Appl. Cryst.* **2005**, *38*, 381–388. [[CrossRef](#)]
48. Sheldrick, G.M. *SHELXL-2014/7, Program for Refinement of Crystal Structures*; University of Göttingen: Göttingen, Germany, 2014.
49. Farrugia, L.J. WinGX suite for small-molecule single-crystal crystallography. *J. Appl. Cryst.* **1999**, *32*, 837–838. [[CrossRef](#)]
50. Bevington, P.R.; Robinson, D.K. *Data Reduction and Error Analysis for the Physical Sciences*; McGraw Hill: New York, NY, USA, 1992; pp. 194–197.
51. OTrott, O.; Olson, A.J. AutoDockVina: Improving the speed and accuracy of docking with a new scoring function, efficient optimization and multithreading. *J. Comput. Chem.* **2010**, *31*, 455–461.
52. Morris, G.M.; Huey, R.; Lindstrom, W.; Sanner, M.F.; Belew, R.K.;Goodsell, D.S.; Olson, A.J. Autodock4 and AutoDockTools4: Automated docking with selective receptor flexibility. *J. Comput. Chem.* **2009**, *16*, 2785–2791. [[CrossRef](#)] [[PubMed](#)]
53. Frisch, M.J.; Trucks, G.W.; Schlegel, H.B.; Scuseria, G.E.; Robb, M.A.; Cheeseman, J.R.; Montgomery, J.A., Jr.; Vreven, T.; Kudin, K.N.; Burant, J.C.; et al. *GAUSSIAN 03 (Revision C.02)*; Gaussian, Inc.: Wallingford, CT, USA, 2004.

